Volume 3, pp. 291-297 (2018)


# Ternary Lead-Chalcogenide Room-Temperature Mid-Wave Infrared Detectors Grown By Spray-Deposition

| | |
|---|---|
| Journal: | *MRS Advances* |
| Manuscript ID | MRSF17-2801680.R1 |
| Manuscript Type: | Symposium EM10 |
| Date Submitted by the Author: | n/a |
| Complete List of Authors: | Abouelkhair, Hussain; University of Central Florida, Physics<br>Figueiredo, Pedro; University of Central Florida, Physics<br>Calhoun, Seth; University of Central Florida, Physics<br>Fredricksen, Chris; University of Central Florida, Physics<br>Oladeji, Isaiah; SISOM THIN FILMS LLC,<br>Smith, Evan; US Air Force Research Laboratory, Sensors Directorate<br>Cleary, Justin; Air Force Research Laboratory, Sensors Directorate<br>Peale, Robert; University of Central Florida, Physics |
| Keywords: | spray deposition, Ir, photoconductivity |
| | |

Volume 3, pp. 291-297 (2018)

# Ternary lead-chalcogenide room-temperature mid-wave infrared detectors grown by spray-deposition

Hussain Abouelkhair,[1] Pedro N. Figueiredo,[1] Seth R. Calhoun,[1] Chris J. Fredricksen,[1] Isaiah O. Oladeji,[2] Evan M. Smith,[3,4] Justin W. Cleary[4] and Robert E. Peale[1]

[1]*Physics, University of Central Florida, Orlando FL 32789, robert.peale@ucf.edu*

[2]*SISOM Thin Films LLC, 1209 W. Gore St. Orlando FL 32805*

[3]*KBRWyle, Beavercreek OH 45431*

[4]*Air Force Research Laboratory, Wright-Patterson AFB OH 45433*

*ABSTRACT*

*Ternary lead chalcogenides, such as $PbS_xSe_{1-x}$, offer the possibility of room-temperature infrared detection with engineered cut-off wavelengths within the important 3-5 micron mid-wave infrared (MWIR) wavelength range. We present growth and characterization of aqueous spray-deposited thin films of PbSSe. Complexing agents in the aqueous medium suppress unwanted homogeneous reactions so that growth occurs only by the heterogeneous reaction on the hydrophilic substrate. The strongly-adherent films are smooth with a mirror-like finish. The films comprise densely packed grains with tens of nm dimensions and a total film thickness of ~400-500 nm. Measured optical constants reveal absorption out to at least 4.5 μm wavelength and a ~0.3 eV bandgap intermediate between those of PbS and PbSe. The semiconducting films are p-type with resistivity ~1 and 85 Ohm-cm at 300 and 80 K, respectively. Sharp x-ray diffraction peaks identify the films as Clausthalite-Galena solid-state solution with a lattice constant that indicates an even mixture of PbS and PbSe. The photoconductive response is observed at both nitrogen and room temperature up to at least 2 kHz chopping frequency.*

## INTRODUCTION

Low-cost, room-temperature mid-wave infrared (MWIR) spectral sensors have application to chemical agent and explosives detection using hand-held devices on small autonomous vehicles. Binary lead-chalcogenide detectors, such as PbS and PbSe are well-established for room temperature operation in the MWIR 3-5 micron wavelength range [1]. PbS has D* exceeding $10^{11}$ cm√Hz/W, but its cut-off wavelength is short of 3 μm. In contrast, the cut-off wavelength of PbSe is 4.6 μm, but its D* is no better than 5 x $10^{10}$ cm√Hz/W. A problem is that these limitations appear to be fundamental to the

Volume 3, pp. 291-297 (2018)

materials, and detector characteristics have not improved significantly in nearly 4 decades, except by optical tricks [2]. An opportunity is ternary lead chalcogenide alloys, such as PbSSe [3], where the high D* and suitable cut-off wavelength of the end members might be achieved simultaneously.

For spectral sensing applications, a range of cut-off wavelengths that span the MWIR is desired. PbS and PbSe have the same crystal structure and form solid solutions. Lattice constant $a$ and bandgap $E_g$ vary monotonically as a function of $x$ in $PbS_xSe_{1-x}$, according to Vegard's law [4]. In its simplest form, $a_{PbSxSe1-x} = x\ a_{PbS} + (1-x)\ a_{PbSe}$, and similarly for $E_g$. This paper reports fabrication and characterization of ternary PbSSe detectors by an aqueous spray deposition method known as Streaming Process for Electrodeless Electrochemical Deposition (SPEED) [5,6]. This method results in strongly adherent, conformal, nano-crystalline thin films that are grown by purely heterogeneous reaction on hydrophilic substrates [5,6]. SPEED is an advance over the chemical bath deposition (CBD) usually used for growth of polycrystalline PbS and PbSe films. SPEED films are more mechanically robust than CBD films. Homogeneous reaction in CBD results mostly in wasteful precipitation and competes with the desired but slower heterogeneous reaction on substrates. CBD films have practical thickness limitations, and they are incompatible with CMOS-type processing due to chemically-induced corrosion. Ternary film growth by CBD is extremely challenging.

SPEED deposits self-assembled nanocrystalline inorganic thin films over large areas, without a vacuum. SPEED has produced operational II-VI semiconductor p-n junction solar cells with efficiency exceeding 10% [7] and solid-state electrolyte for batteries [8]. Growth rates are up to 1 μm/min on hydrophilic rigid or flexible substrates. The de-ionized-water-based precursor is nebulized into 10 - 20 μm droplets and made to impinge on the hydrophilic substrate (metal, glass, oxidized Si, or surface-modified plastics). Water-soluble compounds contain engineered complexing agents that suppress unwanted homogeneous reactions. Growth occurs only by heterogeneous reaction at attached hydroxyl-ions ($OH^-$), which form a high-density monolayer ($>10^{12}$ sites/$cm^2$). Nanocrystals grow at these nucleation sites. Lateral growth is self-limited because the closely-packed grains compete for surface area. $OH^-$ ions are liberated after the reaction, and they repopulate the active sites of the newly created film. Substrate temperatures of 200 – 500 °C accelerate growth, provide the energy needed for the heterogeneous reaction, and volatilize reaction by-products. Powerful ligands and high growth temperature enable growth of binary, ternary, and even quaternary materials. Recrystallization in some cases is accomplished by post-growth annealing.

## EXPERIMENTAL DETAILS

Nanocrystalline PbSSe films were grown on glass and silicon substrates by SPEED. Precursors comprised 0.1 M lead salt in a mixture of deionized water and organic solvents/ligand. Water (70% by volume) acts as a solvent and as the source of the surface-attached $OH^-$ nucleation sites for heterogeneous reaction. The organic solvents ethanol, isopropanol, methyl propanol, and other additional reagents served mainly as complexing agents for Pb ions. The S was supplied by thiourea. Hydrophilic surfaces readily anchor hydroxyl ions that serve as nucleation sites. The $OH^-$ ions attract positively charged complexes to initiate the electrochemical reaction, without external field or electrodes. The heterogeneous chemical reactions are:

Volume 3, pp. 291-297 (2018)

$$[Sub](OH)^- + [PbL_n]^{p+(2+)} \rightarrow [Sub]Pb(OH)^+ + (L_n)^p\uparrow \quad (1)$$

$$[Sub]Pb(OH)^+ + SH^- \rightarrow [Sub]PbS + H_2O\uparrow \quad (2)$$

where L is the ligand supplied by the organic solvents and other complexing agents, [Sub] the heated substrate, p the charge of the ligand L, and n the number of ligands involved in the Pb/L coordination. Up arrows indicate decomposition and evaporation of reaction byproducts. Substrate temperature must exceed the heterogeneous reaction activation energy and be sufficient to eliminate byproducts. Site regeneration follows:

$$[Sub]PbS + OH^- \rightarrow [Sub]PbS(OH)^- \quad (3)$$

The freshly attached $OH^-$ initiates the next growth cycle. The growth temperature is in the range 300 to 500 °C. Se is introduced through post-deposition anneal in nitrogen/Se ambient in a tube furnace at 400 °C. Wet chemically deposited polycrystalline Pb-chalcogenides are sensitive to moisture, UV, and heat [9], but no special precautions controlled these factors for this initial study.

Samples were imaged using a scanning electron microscope (Zeiss ULTRA-55 FEG SEM). Cross sections were also imaged by SEM (Hitachi SU70), and with this instrument energy dispersive x-ray spectroscopy (EDS, EDAX) was used to determine relative film composition using a 5 kV electron beam. Film concentration was analysed as a function of depth using the TEAM EDS software suite to quantify the Pb, Se and S signatures. Accuracy is insufficient for determining absolute atomic concentration, because Pb and S characteristic energies coincide.

Asymmetric out-of-plane X-ray diffraction (PANalytical Empyrean XRD), using the Cu $K\alpha_1$ beam at an incident angle of 10°, determined the crystalline phase and lattice constant. Electrical characterization was performed on films grown on glass. Hot probe determined carrier type, and four-point probe determined resistivity. Resistance was recorded at 300 and 80 K.

IR ellipsometry (JA Woolam, IR-VASE) was used to determine the complex optical constants between 2-15 μm wavelength. The permittivity was modeled by fitting Gaussian oscillators to match the raw ellipsometry data using the Woolam WVASE32 software.

For photoconductivity measurements, a pair of few mm-dimensioned gold contacts separated by ~3 mm on a strip of film ~5 mm wide was deposited by sputtering. This sample was mounted on an aluminum cold finger in a liquid nitrogen optical cryostat with ZnSe window. The sample was illuminated with the unfiltered output of a Xe-arc lamp (ILC Technologies Model 201). The ZnSe window blocks all wavelengths below 500 nm, and the typical infrared output of a Xe lamp drops very quickly beyond 1.1 μm wavelength [10]. That the resulting 0.5 – 1.1 μm wavelength range was responsible for all of the observed photocurrent was confirmed using long-pass filters (Schott glass, silicon, or germanium). The unfocused beam was chopped using a variable speed chopper. A bias of 5 V was applied and the current collected and amplified using a low noise current amplifier (Stanford Instruments SR570) without electronic filtering applied. The output of the current amplifier was input to a digital

Volume 3, pp. 291-297 (2018)

oscilloscope with averaging and peak-to-peak voltage measurement capability. Signal was also observed using a matched load resistor and a voltage preamplifier.

## RESULTS

Figure 1 (left) presents a SEM image of the film surface. Apparent structures with ~20 nm length scale are much smaller than optical wavelengths, which is consistent with the mirror-like surface appearance. Their characteristic size is consistent with the minimum single-crystal grain size for this film determined by XRD peak widths, as shown below. Figure 1 (right) presents a cross-sectional SEM image, giving a film thickness of ~350 nm. Contact profilometry where the film was scratched away from the substrate indicated 450 to 500 nm values. The difference may be due to burr near the edges of the scratch, although the larger thickness is supported by the best fit to ellipsometry data (below). Figure 1 (right) also shows the EDS line scans for the elements Pb, Se and S. Although the concentration ratio values may be inaccurate due to coincidence of Pb and S signals, the ratio of Se to the other elements is uniform throughout the film, showing that Se was well diffused.

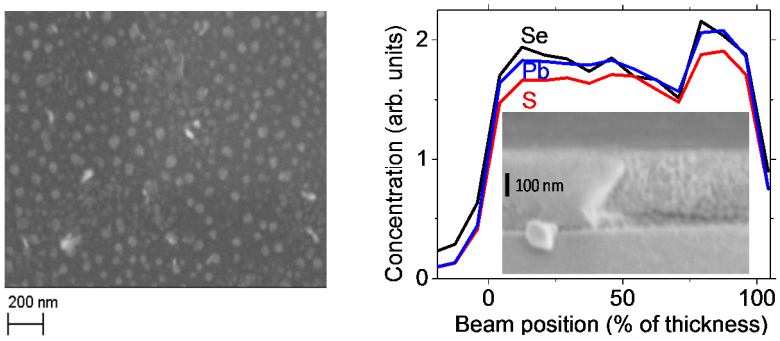


**Figure 1.** (left) SEM image of surface, and (right) cross section and EDS of PbSSe film on glass.

XRD of the film is presented in Figure 2 (left) together with standard references for PbS, PbSe, and $Pb_2SSe$. The sharp peaks are intermediate between those of Clausthalite (PbSe) and Galena (PbS). The determined lattice constant 6.033 Å indicates an even mixture of PbS (5.94 Å) and PbSe (6.12 Å) in solid solution [11, 12]. The full width of the strongest peak is 0.42° for which the Scherrer formula [13] indicates a minimum single-crystal grain size of 22 nm. This is consistent with the structure seen in the SEM image, Figure 1.

Figure 2 (right) presents infrared spectra of the complex permittivity $\varepsilon' + i\,\varepsilon''$. The fit to the ellipsometric spectrum was best assuming a thickness of 506 nm. The thickness parameter was weakly correlated with the resulting permittivity in the model fitting. Complex refractive index, with real and imaginary parts n and κ, was calculated from these data using standard formulas [14]. The infrared refractive index beyond a wavelength of 6 μm was found to have the value n ~ 3.35. This value is less than for either PbS (3.9) or PbSe (4.8), which suggests film porosity. The absorption coefficient α was calculated from the extinction coefficient κ according to [14] $\alpha = 4\pi\kappa/\lambda$, and its

Volume 3, pp. 291-297 (2018)

spectrum is plotted in Figure 2 (right). Significant absorption is observed out to 4.5 μm wavelength, where an optical depth of unity would be achieved with a 1 μm thick film. Isolated absorption features of unknown origin occur at 7.9 and 9.6 μm.

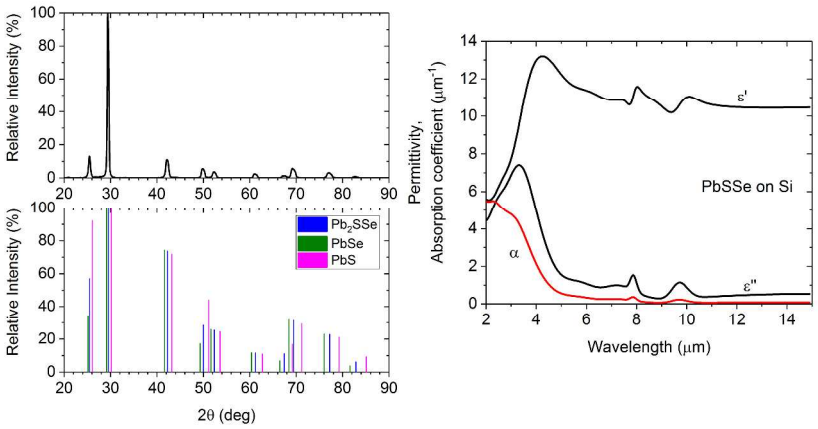


**Figure 2**. (left) XRD, and (right) permittivity and absorption coefficient spectra of PbSSe film.

Figure 3 (left) presents the square of the absorption coefficient as a function of energy. The direct-gap fundamental absorption coefficient spectrum is proportional to $\sqrt{(h\nu - E_g)}$, where the first term is photon energy and the second is the direct band gap [15,16]. Extrapolation of the dominant linear portion of the spectrum in Figure 3 to zero absorption gives $E_g = 0.30$ eV for the film. This value is intermediate between the values indicated in Figure 3 for PbS (0.37 eV) and PbSe (0.27 eV), though it is closer to the latter value. Assuming Vegard's law, this suggests that our sample is $Pb_2S_{0.3}Se_{0.7}$, in contrast to the $Pb_2S_{0.5}Se_{0.5}$ composition determined from XRD.

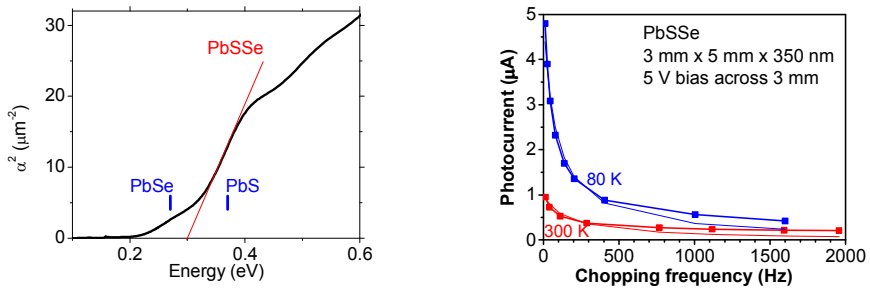


**Figure 3**. (left). Square of absorption coefficient vs. photon energy for the PbSSe film. (right) Measured current responsivity as a function of chopping frequency at 80 K and 300 K. The thin solid lines are fits of Eq. (4) to the low frequency part of the data.

The grown films are p-type with resistivity 1.2 Ω-cm as determined by 4-pt probe method. The resistance of the sample prepared for photoconductivity was 39 kΩ and 1.5 MΩ at 300 and 80 K, respectively. From, sample dimensions and contact

Volume 3, pp. 291-297 (2018)

separation, we calculate resistivities of 2.2 and 85 Ω-cm, respectively. The room temperature value is about twice higher than the 4-point probe value, suggesting contributions from contact and lead resistance. Assuming these to be temperature independent, their contribution to the low temperature resistivity must be small.

Figure 3 (right) presents the photoconductive response of the PbSSe film. Photoconductive response should follow the function

$$R = \frac{R_o}{\sqrt{1+(2\pi\tau f)^2}} \quad (4)$$

where *f* is the chopping frequency [17]. Fits of Equation 4 to the low frequency part of the data are represented by the thin lines. The 80 and 300 K parameter values ($R_0$, $\tau$) were (5 μA, 2 ms) and (1 μA, 1 ms), respectively. A non-linear least squares fit to the entire frequency range gives a worse looking fit at low chopping frequencies. The data differ from Equation 4 by having a long tail of persisting photoresponse up to at least 2 kHz. The photoresponse drops fivefold when the sample is warmed from 80 to 300 K, and the response time from the fit drops twice. The dark current increases to about 100 μA at room temperature, which is adequately explained by the 85x drop in resistance.

## CONCLUSIONS

This paper reported physical and optical characteristics of thin PbSSe films grown by aqueous spray deposition of nano-crystalline PbS followed by Se diffusion. Room-temperature photoconductivity up to 2 kHz chopping frequency was observed. Considerable improvement is expected with post-growth processing and optimization.

## References


1. W. L. Wolfe and G. J. Zissis, editors, *The Infrared Handbook* (Office of Naval Research, Arlington VA 1978), Chapter 11.
2. B. Weng, J. Qiu, Z. Yuan, P. R. Larson, G. W. Strout, and Z. Shi, Appl. Phys. Lett. **104**, 021109 (2014).
3. N. K. Abbas, E. M. Al-Fawade and S. J. Alatya, J. Mat. Sci. Eng. **A 3**, 82 (2013).
4. L. Vegard, Zeitschrift für Physik **5**, 17 (1921).
5. F. Khalilzadeh-Rezaie, I. O. Oladeji, J. W. Cleary, N. Nader, J. Nath, I. Rezadad, and R. E. Peale, Optical Materials Express **5**, 2184 (2015).
6. R. E. Peale, E. Smith, H. Abouelkhair, I. O. Oladeji, S. Vangala, T. Cooper, G. Grzybowski, F. Khalilzadeh-Rezaie, J. W. Cleary. Opt. Eng. **56**, 037109 (2017).
7. I. O. Oladeji, L. Chow, C. S. Ferekides, V. Viswana than, Z. Zhao, Solar Energy Materials & Solar Cells Lett. **61**, 203 (2000).
8. I. O. Oladeji, US Patent 0168327 (2011).
9. Brian Elias, Proc. SENSOR+TEST Conference 2009 - IRS² (2009).
10. Cermax® Xenon Lamp Engineering Guide (Excelitas Technologies Corp. 2011).
11. Dr. H. Berger, Dr. H.-H. Niebsch and Dr. A. Szczerbakow, Crystal Research and Technology 20, K8 (1985).

Volume 3, pp. 291-297 (2018)

12. R. G. Coleman, Am. Mineralogist **44**, 166 (1959).
13. A. Patterson, Phys. Rev. **56**, 978 (1939).
14. L. D. Landau, E. M. Lifshitz, and L. P. Pitaevskii, *Electrodynamics of Continuous Media*, 2nd edition, (Elsevier Butterworth Heineman 1984) Section 83.
15. J. I. Pankove, *Optical Processes in Semiconductors* (Dover 1971), Chapter 3.
16. T. S. Moss, *Optical Properties of Semi-conductors* (Butterworths Scientific, London, 1959), Chapter 3.
17. E. L. Dereniak and G. D. Boreman, *Infrared Detectors and Systems* (John Wiley and Sons, New York, 1996).